Isoscalar E0,E1,E2, and E3 strength in ^{92,96,98,100}Mo

D. H. Youngblood, Y.-W. Lui, Krishichayan, J. Button, G. Bonasera, and S. Shlomo

Phys. Rev. C **92**, 014318 — Published 23 July 2015

DOI: 10.1103/PhysRevC.92.014318

Isoscalar E0, E1, E2, and E3 Strength in ^{92,96,98,100}Mo

D. H. Youngblood[1], Y. -W. Lui[1], Krishichayan[2,3], J. Button[1], G. Bonasera[1] and S. Shlomo[1]

[1]Cyclotron Institute, Texas A&M University, College Station, Texas 77843, USA.
[2]Department of Physics, Duke University, Durham, North Carolina 27708, USA.
[3]Triangle Universities Nuclear Laboratory, Durham, North Carolina 27708, USA.

ABSTRACT

Isoscalar giant resonances in ^{92,96,98,100}Mo have been studied with inelastic scattering of 240 MeV α particles at small angles including 0^o. A significant fraction of the EWSR was found for isoscalar E0 (107%, 105%, 103%, 110%), E1(71%, 71%, 70%, 55%), E2(73%, 69%, 85%, 79%) and high energy octupole E3(52%, 65%, 61%, 53%) resonances in ^{92,96,98,100}Mo, respectively. Spherical Hartree-Fock-based random-phase approximation calculations were made for each multipole using the KDE0v1 Skyrme-type effective interaction and the results are compared to the experimental distributions.

PACS number(s): 25.55.Ci,24.30.Cz,27.60.+j

I. Introduction

The isoscalar giant resonances in the Mo isotopes have received limited study. Moalem *et al.* [1] studied the isoscalar giant quadrupole resonance (GQR) with inelastic scattering of 110 MeV ^{3}He in all of the stable Mo isotopes while Duhamel *et al.* [2] reported results for the GQR and the isoscalar giant monopole resonance(GMR) in ^{92}Mo obtained by inelastic scattering of 152 MeV α particles. These analyses assumed Gaussian shapes for both the GQR and GMR distributions. Recently, we reported a study using inelastic scattering of 240 MeV α particles at small angles including 0^o of the GMR in the Zr and Mo isotopes [3] where the E0 strength has two components. Because

of the excellent peak-to-continuum ratio [4] with the 240-MeV α data, the actual distribution of strength between E_x = 9 and 36 MeV can be obtained not only for the GMR, but for the Isoscalar Giant Dipole resonance (ISGDR), the GQR, and the High Enegry Octupole Resonance (HEOR) as well. In this paper we report E1, E2, and E3 multipole strength distributions obtained for ^{92,96,98,100}Mo and compare the results of spherical Hartree-Fock (HF)-based random-phase-approximation (RPA) calculations [5] with the KDE0v1 Skyrme-type effective interaction [6].

II. Experimental Technique and Data Analysis

The experimental technique and detailed method of the analysis have been discussed thoroughly in Ref. [4] and are summarized only briefly below. A beam of 240-MeV α particles from the Texas A&M K500 superconducting cyclotron, after passing through a beam analysis system, bombarded self-supporting target foils 5-8 mg/cm^2 thick enriched to more than 96% in the desired isotope located in the scattering chamber of the multipole-dipole-multipole (MDM) spectrometer. The horizontal and vertical acceptance of the spectrometer were set at 4º. Scattered particles entering the MDM spectrometer were momentum-analyzed and measured by a 60 cm long focal plane detector, which consisted of four resistive wire proportional counters to measure position, as well as an ionization chamber to provide ΔE and a plastic scintillator behind the ionization chamber to measure the energy deposited and provide a fast timing signal for the event trigger.

The data for each run were binned into ten angle bins by horizontal angle. The differential cross section was extracted from the number of beam particles collected, the target thickness, the solid angle, the yields measured, and the dead time. The number of beam particles was monitored with a detector at a fixed scattering angle in the scattering chamber. Dead time of the data acquisition system was measured by comparing the number of pulses sent to the system to those accepted. The cumulative uncertainties in the above parameters result in an approximately ±10% uncertainty in absolute cross sections. ^{24}Mg spectra were taken before and after each run, and the 13.85 ± 0.02 MeV L = 0 state [7] was used as a check on the energy calibration in the giant resonance region.

Giant resonance data were taken with the spectrometer at 0.0^o ($0.0^o < \theta < 2.0^o$) and at 4.0^o ($2.0^o < \theta < 6.0^o$). Sample spectra obtained for ^{92,96,98,100}Mo are shown in Fig. 1. The giant resonance peaks can be seen extending up past E_x = 30 MeV in all nuclei. The spectra were divided into a peak and a continuum where the continuum was assumed to have the shape of a straight line at high excitation joining onto a Fermi shape at low excitation to model particle threshold effects [4]. Samples of the continua used in the analysis are also shown in Fig. 1.

III. Multipole Analysis

The multipole components of the giant resonance peak were obtained [4] by dividing the peak into multiple regions (bins) by excitation energy and then comparing the angular distributions obtained for each of these bins to the sum of those calculated for isoscalar 0^+,1^-,2^+,3^- and 4^+ transitions and the isovector 1^- excitation with distorted wave Born approximation (DWBA) calculations. Fits to the angular distributions were carried out with a sum of isoscalar 0^+, 1^-, 2^+, 3^-, and 4^+ strengths. The isovector giant dipole resonance contributions were calculated from the known distribution [8] and were held fixed in the fits. The uncertainty from the multipole fits was determined for each multipole by incrementing (or decrementing) that strength, then adjusting the strengths of the multipoles to minimize total χ^2. This continued until the new χ^2 was one unit larger than the total χ^2 obtained for the best fit.

The DWBA calculations were performed [9,10] using the density-dependent single-folding model for the real part, obtained with a Gaussian α-nucleon potential, and a phenomenological Woods-Saxon potential for the imaginary term. These calculations were carried out with the code PTOLEMY [11]. Optical parameters used for the calculations were those determined for elastic scattering of 240 MeV α particles from ^{90}Zr [12] and are given in Table I. The Fermi parameters used for the density distribution of the nuclear ground state were obtained from Ref. [13].

Table I. Optical parameters used in DWBA calculations.

V (MeV)	W_i (MeV)	r_i (fm)	a_i (fm)

40.2	40.9	0.786	1.242

The shape of the real part of the potential and the form factors for PTOLEMY were obtained using the codes SDOLFIN and DOLFIN [14]. The transition densities and sum rules for various multipolarities are discussed thoroughly in Ref. [15] and, except for the ISGDR, the same expressions and techniques were used in this work. The transition density for inelastic alpha-particle excitation of the ISGDR given by Harakeh and Dieperink [16] (and described in Ref. [15]) is for only one magnetic substate, so that the transition density given in Ref. [15] must be multiplied by $\sqrt{3}$ in the DWBA calculations.

Samples of the angular distributions obtained for the giant resonance peak and the continuum are shown for ^{92}Mo in Fig. 2 and for ^{98}Mo in Fig. 3. Distributions for ^{96}Mo and ^{100}Mo are similar. Sample fits obtained, along with the individual components of the fits, are shown superimposed on the data in Figs. 2 and 3. The continuum distributions are similar over the entire energy range, whereas the angular distributions of the cross sections for the peak change as the contributions of different multipoles dominate in different energy regions.

Several analyses were carried out to assess the effects of different choices of the continuum on the resulting multipole distribution, as described in Ref. [17], where the continuum was systematically varied and the data were reanalyzed. The strength distributions obtained from these analyses using different choices of continuum were then averaged and errors were calculated by adding the errors obtained from the multipole fits in quadrature to the standard deviations between the analyses with different continua. The resulting E0-E3 multipole distributions obtained for ^{92}Mo, ^{96}Mo, ^{98}Mo and ^{100}Mo are shown in Figs. 4 and 5.

IV. Description of Microscopic Calculations

The microscopic mean-field based RPA theory provides a good description of collective states in nuclei [18,19]. It is common to calculate the RPA states $|n\rangle$ with the corresponding energies E_n, and obtain the strength (response) function

$$S(E) = \Sigma_n |\langle 0|F|n\rangle|^2 \delta(E-E_n),$$

for a certain single particle scattering operator F = Σ f(i), and then determine the energy moments

$$m_k = \int E^k S(E)\, dE.$$

The constrained energy, E_{con}, centroid energy, E_{cen}, and the scaling energy, E_{scal}, of the resonance are then obtained from:

$E_{con} = (m_1/m_{-1})^{1/2}$, $E_{cen} = m_1/m_0$, $E_{scal} = (m_3/m_1)^{1/2}$.

The energy moment m_1 can also be calculated using the Hartree-Fock (HF) ground state wave function, leading to an energy weighted sum rule (EWSR).

In a fully self-consistent mean-field calculation of the response function, one adopts an effective two-nucleon interaction V, usually fitted to ground states properties of nuclei, and determines the HF mean-field. Then, the RPA calculation is carried out with all the components of the two-body interaction using a large configuration space. Employing the numerical approach of [5, 20], we have carried out spherical HF based RPA calculations of the strength functions and centroid energies of the isoscalar (T=0) giant resonances in ^{92,96,98,100}Mo by employing an occupation number approximation for the single particle orbits of the open shell nuclei. For the single-particle scattering operator, $F = \sum_i f(r_i)Y_{L0}$, we used $f(r) = r^2$ for the Monopole (L=0) and Quadrupole (L=2), $f(r) = r^3$ for the Octopole (L=3), and $f(r) = r^3 - \frac{5}{3}\langle r^2 \rangle r$ for the Dipole (L=1) in order to account for contribution from the spurious state [21,22]. Here we present results obtained using the KDE0v1 Skyrme-type effective interaction, which was fitted to ground state properties of nuclei such as binding energy and radii as well as the breathing mode energies of several nuclei[6]. The energy moments of the calculated strength functions were obtained using small smearing widths (0.1 MeV) to insure accuracy and they are given in Tables II-V. We used the appropriate experimental excitation energy ranges: ISGMR, 9 – 36 MeV, low component of the ISGDR, 9 – 20 MeV, high component of the ISGDR, 20 – 36 MeV, ISGQR, 9 – 36 MeV, and ISGOR, 15 – 36 MeV when calculating these moments. The calculated distributions, using smearing widths of Γ = 10 MeV for the ISGDR and Γ = 5 MeV for the other multipoles, are shown superimposed on the experimental results in Figs. 4 and 5.

V. Discussion

The E0-E3 multipole distributions obtained for ^{92}Mo, ^{96}Mo, ^{98}Mo and ^{100}Mo are shown in Figs. 4 and 5 along with two (Gaussian) peak fits for the E0 and E1 distributions, while single Gaussian fits are shown for each of the E2 distributions and the E3 distributions for ^{96}Mo, ^{98}Mo and ^{100}Mo. The E0 distributions have been reported previously [3] and the implications of these distributions, along with those of the Zr isotopes were explored. Parameters obtained for the moments of the multipole distributions and/or from the Gaussian fits are given in Tables II-V along with those obtained from the KDE0v1 calculations. Each multipole is discussed separately below.

A. E0 strength

The E0 distributions obtained for the four Mo isotopes have been previously reported [3] and are shown in Figs. 4 and 5. The parameters obtained are summarized in Table II. Each consists of an approximately symmetrical peak between 15.7- 16.8 MeV, with a tail extending up to 30-35 MeV. Also shown in the figures are two-peak fits to the distributions. The E0 energy-weighted sum rule (EWSR) strengths obtained are 107±13%, 105±12%, 103±12%, and 110±12% respectively for ^{92,96,98,100}Mo. The existence of this high energy tail (or second peak) was the focus of Ref. [3], but its origin is not understood. The substantial enhancement of the strength in the tail to that in the lower symmetrical peak in both ^{92}Mo and ^{92}Zr results in K_A values for these two nuclei 8σ and 4σ above those obtained with interactions that predict K_A values in agreement with those for the other Zr and Mo isotopes [3]. The results of HF-RPA calculations for the E0 strength (broadened with a Lorentzian shape with ~ 5 MeV width) are shown superimposed on the data in Figs. 4 and 5. The calculations for each isotope result in a single slightly asymmetrical peak concentrated in a narrow band just above the narrow peak in the data. The energies obtained for the 4 Mo isotopes from the two peak fits for the low and high components of the E0 distributions are plotted versus A in Fig. 6. Also shown are lines representing $74/A^{1/3}$ and $109/A^{1/3}$ on the low and high plots indicating a possible $A^{-1/3}$ dependence of the energies. The energy of the higher peak is essentially

constant (within errors) over the mass range 92-100, however the errors are large enough to possibly mask an $A^{-1/3}$ dependence. The energy of the lower peak clearly decreases somewhat faster than $A^{-1/3}$.

B. Isoscalar E1 strength

Much of the expected isoscalar E1 strength was identified in the Mo isotopes with strength corresponding to 71±8%, 71±8%, 70±8%, and 55±7% of the isoscalar E1 EWSR located in ^{92}Mo, ^{96}Mo, ^{98}Mo, and ^{100}Mo respectively between E_x=9- 36 MeV. The isoscalar dipole is split into $1\hbar\omega$ and $3\hbar\omega$ components [23-25] and the upper component is expected to be a compression mode whose energy is related to the compression modulus K_A of the nucleus. Two-peak Guassian fits were made to the distributions shown in Figs. 4 and 5. The fits are shown in the figures and the parameters obtained are listed in Table III. There are no previous reports of the ISGDR in the Mo isotopes. HF-RPA calculations with the KDE0v1 interaction are shown superimposed on the multipole distributions in Figs. 4 and 5. The HF-RPA calculations show 14-15% of the ISGDR EWSR in the range E_x=9-20 MeV (mostly the $1\hbar\omega$ component) with m_1/m_0~14 MeV and 69-76% of the ISGDR EWSR in the range E_x=20-36 MeV (the $3\hbar\omega$ component) with m_1/m_0 ~28.5 MeV. For ^{92}Mo and ^{98}Mo, the strongest peak in the calculation is at approximately E_x=32.5-33 MeV whereas the data peak around 26-28 MeV and are substantially lower than the calculation in the 34-36 MeV region. For ^{96}Mo and ^{100}Mo the experimental and calculated distributions are in fairly good agreement (within the errors) though the strength seen in ^{100}Mo is a little low. The strengths and Gaussian centroids of the high energy peaks are compared to those obtained from the HF-RPA calculations in Table III and Fig. 7. Except for ^{96}Mo, the strength seen experimentally is somewhat less than predicted to lie in this energy range.

C. E2 strength

The E2 strengths in ^{92}Mo, ^{96}Mo, ^{98}Mo and ^{100}Mo, summarized in Table IV, are concentrated in (almost) Gaussian peaks centered between 13.5 and 14.2 MeV containing 73±13%, 69±13%, 85±14%, and 79±14% of the E2 EWSR, respectively. The peaks were fitted with Gaussians and m_1/m_0, the RMS width, and the Gaussian parameters are

given. The peaks are a little asymmetric with extra yield on the low energy side, so the Gaussian energies are a few hundred keV higher than m_1/m_0. Moalem *et al.* [1] measured the GQR in ^{92,94,96,98,100}Mo with inelastic scattering of 110 MeV ^{3}He and our results for %EWSR, energy, and width agree within the errors with their work. Duhamel *et al.* [2] measured the GQR in ^{92}Mo with inelastic scattering of 120 MeV α particles and obtained an energy and width in agreement with our result, but only identified 23±5% of the E2 EWSR strength. Fig. 8 compares the (Gaussian) energy of the GQR in the Mo isotopes obtained from the 3 experiments and m_1/m_0 obtained from the calculation with the KDE0v1 interaction. The calculated energies are ~ 1 MeV higher than our experimental energies. The position of the GQR is sensitive [26] to the effective mass (0.74 in KDE0v1), and a higher effective mass would lower the predicted GQR energy, obtaining agreement with data with effective mass of ~ 0.8, see Ref. [27] for a more detailed investigation.

D. E3 strength

In the harmonic oscillator shell model, E3 strength in a nucleus is split into a $1\hbar\omega$ Low-Energy-Octupole-Resonance (LEOR) containing 25% of the isoscalar E3 EWSR and a $3\hbar\omega$ HEOR containing 75% of the EWSR [28], however coupling these modes with an octupole-octupole residual interaction results in the LEOR having ~ 35% of the E3 EWSR and the HEOR having ~ 65%. Our low energy cutoff in this experiment lies in the middle to higher region of the LEOR, so that we are unable to extract useful parameters for the LEOR. The observed E3 strength distributions (Figs. 4 and 5) are broadly spread from E_x ~ 9 MeV (the lower threshold of our detector) and tapering off between E_x =30-35 MeV before reaching the upper limit of the region we observe (E_x ~36 MeV). We arbitrarily assign to the HEOR that strength lying above E_x=12-15 MeV depending on the apparent gap in the strength distributions, and the strengths, m_1/m_0 and RMS widths for the data above this division are listed in Table V along with m_1/m_0 and the strengths calculated with KDE0v1 over the range 15-36 MeV. There are no previous reports of the HEOR in the Mo isotopes. The isoscalar E3 strength calculated with the KDE0v1 interaction is also shown in Figs. 4 and 5 and has peaks at ~ 8 MeV (the LEOR) and at ~ 29 MeV (the HEOR) whereas the experimental strength lies in a broad

peak centered at ~ 21.5 MeV. The experimental and calculated energies and strengths are compared in Fig. 9. The excitation energy (m_1/m_0) we obtain for each of the isotopes is near 21.5 MeV, well below the ~26.1-27.0 MeV obtained with the HF-RPA calculations. The centroid (m_1/m_0) obtained from the HF-RPA calculations for the strength lying above E_x=15 MeV of the E3 is 2-3 MeV below the ~ 29 MeV peak position because there is significant strength in the 15-20 MeV range. The strengths obtained for the HEOR in the HF-RPA calculations range from 60.7-63.9% of the E3 EWSR, in agreement within the errors with data for ^{96}Mo and ^{98}Mo. The observed E3 strengths for ^{92}Mo (52±7%) and ^{100}Mo (53±7%) are somewhat lower than the 63.85% and 61.80% obtained with the KDE0v1 interaction. The energies of the HEOR and the GQR are sensitive to the effective mass [26], and a larger effective mass would result in a lower energy for both these excitations.

VI. Summary

We have obtained distributions for isoscalar E0, E1, E2, and E3 strength containing 52-110% of the expected strength in ^{92}Mo, ^{96}Mo, ^{98}Mo, and ^{100}Mo and compared these to spherical Hartree-Fock-RPA calculations using the KDE0v1 Skyrme type interaction. As discussed in a previous report [3], the E0 strength has a high energy tail which contains a substantially larger fraction of the E0 strength in ^{92}Mo than the other isotopes which shifts the GMR energy substantially higher for ^{92}Mo, a shift not seen in the HF-RPA calculation. The source of this "tail", not present in heavier nuclei, is not understood, and the distributions for the other multipoles do not differ substantially between the isotopes. The position of the high energy part of the isoscalar dipole agrees reasonably well with the HF-RPA calculation. The position, strength, and width of the E2 distributions agree within errors with those obtained by Moalem *et al*. [1], but are ~1 MeV below those obtained with the HF-RPA calculations. The HEOR strength lies in a broad peak centered at ~ 21.5 MeV in each isotope, approximately 4 MeV below that obtained with the HF-RPA calculations. We will follow up with a study, similar to an earlier one for ^{40}Ca and ^{48}Ca [26] which found the E2 and E3 centroids most sensitive to

the effective mass m*/m by carrying out self-consistent HF-RPA calculations using a number of interactions.

Acknowledgments

This work was supported in part by the U.S. Department of Energy under grant DE-FG03-93ER40773.

References

1. A. Moalem, Y. Gaillard, A. M. Bemolle, M. Buenerd, J. Chauvin, G. Duhamel, D. Lebrun, P. Martin, G. Perrin, and P. de Saintignon, Phys. Rev. C **20**, 1593(R) (1979).

2. G. Duhamel, M. Buenerd, P. de Saintignon, J. Chauvin, D. Lebrun, Ph. Martin, and G. Perrin, Phys. Rev. C **38**, 2509 (1988).

3. D. H. Youngblood, Y. -W. Lui, Krishichayan, J. Button, M. R. Anders, M. L. Gozelik, M. H. Urin and S. Shlomo, Phys. Rev. C **88**, 021301(R) (2013).

4. D. H. Youngblood, Y. -W. Lui and H. L. Clark, Phys. Rev. C **65**, 034302 (2002); **63**, 067301 (2001); **61**, 067307 (2000);**60**, 014304 (1999).

5. P. -G. Reinhardt, Ann. Phys. (Leipzig) **1**, 632 (1992).

6. B. K. Agrawal, S. Shlomo, and V. K. Au, Phys. Rev. C **72**, 014310 (2005).

7. K. van der Borg, M. N. Harakeh, and A. van der Woude, Nucl. Phys. **A365**, 243 (1981).

8. S. S. Dietrich and B. L. Berman, At. Data Nucl. Data Tables **38**, 199 (1988).

9. G. R. Satchler and Dao T. Khoa, Phys. Rev. C **55**, 285 (1997).

10. H. L. Clark, Y. -W. Lui, and D. H. Youngblood, Phys. Rev. C **57**, 2887 (1998).

11. M. Rhoades-Brown, M. H. Macfarlane, and S. C. Pieper, Phys. Rev. C **21**, 2417 (1980); M. H. Macfarlane and S. C. Pieper, Argonne National Laboratory Report No. ANL-76-11, 1978 (unpublished).

12. H. L. Clark, Y. -W. Lui, and D. H. Youngblood, Nucl. Phys. **A687**, 80c (2000).

13. G. Fricke, C. Bernhardt, K. Heilig, L. A. Schaller, L. Schellenberg, E. B. Shera, and C. W. Jager, Atomic and Nuclear Data Tables **60**, 177 (1995).

14. L. D. Rickerston, The folding program DOLFIN, 1976 (unpublished).

15. D. H. Youngblood, Y. -W. Lui, and H. L. Clark, Phys. Rev. C **55**, 2811 (1997).

16. M. N. Harakeh and A. E. L. Diepernik, Phys. Rev. C **23**, 2329 (1981).

17. D. H. Youngblood, Y. -W. Lui, H. L. Clark, B. John, Y. Tokimoto, and X. Chen, Phys. Rev. C**69**, 034315 (2004).

18. A. Bohr and B. M. Mottelson, *Nuclear Structure II, (Benjamin, New York, 1975).*

19. S. Shlomo, V. M. Kolomietz, and G. Colo, Eur. Phys. J. **A30**, 23 (2006) and references therein.

20. Tapas Sil, S. Shlomo, B. K. Agrwal, and P. G. Reinhard, Phys. Rev. C **73**, 034316 (2006).
21. S. Shlomo and A. I. Sanzhur, Phys. Rev. C **65**, 044310 (2002).
22. B. K. Agrawal, S. Shlomo, and A. I. Sanzhur, Phys. Rev. C **67**, 034314 (2003).
23. H. L. Clark, Y.-W. Lui, and D. H. Youngblood, Phys. Rev. C **63**, 031301(R) (2001).
24. G. Colo, N. Van Giai, P. F. Bortignon, and M. R. Quaglia, Phys. Lett. B **485**, 362 (2000).
25. D. Vretenar, A. Wandelt, and P. Ring, Phys. Lett. B **487**, 334 (2000).
26. M. Anders, S. Shlomo, Tapas Sil, D. H. Youngblood, Y.-W. Lui, and Krishichayan, Phys. Rev. C **87**, 024303 (2013).
27. G. Bonasera *et al.* (to be published).
28. J. M. Moss, D. H. Youngblood, C. M. Rozsa, D. R. Brown, and J. D. Bronson, Phys. Rev. Lett. **37**, 816 (1976).

Figure Captions

Fig. 1. (Color online) Inelastic α spectra obtained at two angles for ^{92,96,98,100}Mo. The thick pink lines show a continuum chosen for the analysis.

Fig. 2. (Color online) The angular distributions of the ^{92}Mo cross sections for a 500 keV wide bin centered at the excitation energy (in MeV) indicated in each panel for inelastic α scattering for three excitation ranges of the GR peak and the continuum. The lines through the data points indicate the multipole fits. Contributions of each multipole are shown (L=0 red, L=1 T=0 blue-green, L=1 T=1 blue, L=2 maroon, L=3 brown, L=4 green). The statistical errors are shown, but in many cases are smaller than the data points.

Fig. 3. (Color online) The angular distributions of the ^{98}Mo cross sections. See Fig. 2 caption.

Fig. 4. (Color online) Strength distributions obtained for ^{92}Mo and ^{96}Mo are shown by the histograms. Error bars represent the uncertainty due to the fitting of the angular distributions and different choices of the continuum as described in the text. The thick lines in the E0 and E1 distributions represent the individual peaks and their sum obtained from the Gaussian fits (the blue and yellow lines are the individual peaks, while the brown line indicates the sum). The thin (red) lines are the strength distributions obtained with the HF-RPA calculations using the KDE0v1 interaction, smeared to more closely represent the data as discussed in the text.

Fig. 5. (Color online) Strength distributions obtained for ^{98,100}Mo are shown by the histograms. See Fig.4 caption.

Fig. 6. (Color online) The centroids of the Gaussians obtained from the fits to the E0 distributions for the Mo isotopes are plotted vs. A. The error bars indicate the uncertainty obtained using the errors shown in Figs. 4 and 5. The (yellow) lines show (a) $74*A^{-1/3}$ and (b) $109*A^{-1/3}$ in two plots.

Fig. 7. (Color online) The centroid of the Gaussian fit to the high energy peak in the ISGDR distributions for each of the Mo isotopes is plotted vs. A. in (a) while the strength of the upper peak is plotted in (b). The error bars indicate the uncertainty obtained using the errors shown in Figs. 4 and 5. The triangles (blue) show m_1/m_0 and the strength between E_x=20 MeV and E_x=36 MeV calculated with HF-RPA using the KDE0v1 interaction.

Fig. 8. (Color online) The centroid of the E2 strength in each of the Mo isotopes obtained in this work [red squares] is plotted vs. A. The error bars indicate the uncertainty obtained using the errors shown in Figs. 4 and 5. Also shown with error bars are centroids reported in Ref. [1] (black diamonds) and a measurement for ^{92}Mo [2] (blue circle). The light blue triangles show the centroid of the E2 strength obtained from HF-RPA calculations with the KDE0v1 interaction.

Fig. 9. (Color online) The centroid of the E3 strength observed above E_x=15 MeV for each of the Mo isotopes in this work [red squares] is plotted vs. A in (a), while the strength in this region is plotted in (b). The error bars indicate the uncertainty obtained using the errors shown in Figs. 4 and 5. The large light blue triangles show (a) the centroid and (b) the % EWSR of the E3 strength between E_x=15 MeV and E_x=36 MeV obtained from HF-RPA calculations with the KDE0v1 interaction.

Table II. Parameters obtained for the E0 distributions shown in Figs. 4 and 5. Uncertainties include systematic errors.

				Gaussian Fit							
				Low Peak					High Peak	KDE0v1	
	% E0	$(m_3/m_1)^{1/2}$	m_1/m_0	E_x	Γ	% E0	E_x	Γ	% E0	$(m_3/m_1)^{1/2}$	% E0
Nucleus	EWSR	(MeV)	(MeV)	(MeV)	(MeV)	EWSR	(MeV)	(MeV)	EWSR	(MeV)	EWSR
^{92}Mo	107±13	$21.68^{+0.53}_{-0.33}$	$19.62^{+0.28}_{-0.19}$	16.8	4	42	23.9	14.7	65	18.51	99.43
^{96}Mo	105±12	$18.18^{+0.20}_{-0.13}$	$16.95^{+0.12}_{-0.10}$	16.4	5.7	83	23.8	5.7	20	18.04	98.36
^{98}Mo	103±12	$17.29^{+0.46}_{-0.21}$	$16.01^{+0.19}_{-0.13}$	15.7	6.5	89	24.2	5.6	14	18.07	98.10
^{100}Mo	110±12	$17.35^{+0.16}_{-0.12}$	$16.13^{+0.11}_{-0.10}$	15.8	7.1	97	23.6	5.5	14	17.89	99.28

Table III. Parameters obtained for the isoscalar E1 distributions shown in Figs. 4 and 5. Uncertainties include systematic errors.

		Gaussian Fit						Low Peak		High Peak	
	Total	Low Peak			High Peak			KDE0v1	% E1	KDE0v1	% E1
	% E1	E_x	Γ	% E1	E_x	Γ	% E1	m_1/m_0	EWSR	m_1/m_0	EWSR
Nucleus	EWSR	(MeV)	(MeV)	EWSR	(MeV)	(MeV)	EWSR	(MeV)		(MeV)	
^{92}Mo	71±8	17.5±0.4	5.4±0.7	5.8±1.1	27.6±0.5	10.2±2.0	59±7	13.46	13.95	28.81	75.58
^{96}Mo	71±8	15.9±0.3	10.1±1.1	17±2	30.0±0.7	13.1±2.9	62±8	14.30	15.05	28.37	69.22
^{98}Mo	70±8	16.0±0.3	10.9±1.1	26±3	27.4±0.7	10.8±3.0	49±8	14.02	15.06	28.36	70.01
^{100}Mo	55±7	13.0±0.3	11.6±1.2	18±3	30.1±0.7	12.5±3.8	47±10	14.50	13.99	28.37	71.10

Table IV. Parameters obtained for the isoscalar E2 distributions shown in Figs. 4 and 5. Uncertainties include systematic errors.

				Gaussian Fit		KDE0v1	
Nucleus	% E2 EWSR	m_1/m_0 (MeV)	RMS width (MeV)	E_x (MeV)	Γ (MeV)	m_1/m_0 (MeV)	% E2 EWSR
^{92}Mo	73±13	14.16±0.25	2.03±0.30	14.51±0.23	4.84±0.35	15.44	93.48
^{96}Mo	69±13	13.61±0.24	1.80±0.25	13.85±0.25	4.70±0.37	14.78	97.18
^{98}Mo	85±14	13.53±0.23	2.80±0.26	13.85±0.24	4.68±0.34	14.77	97.45
^{100}Mo	79±14	13.46±0.26	1.91±0.26	13.60±0.26	4.75±0.38	14.76	97.18

	Ref. 1			Ref. 2		
Nucleus	% E2 EWSR	E_x (MeV)	Γ (MeV)	% E2 EWSR	E_x (MeV)	Γ (MeV)
^{92}Mo	84±17	15.1±0.4	5.0±0.4	23±5	14.1±0.2	4.55±0.34
^{96}Mo	72±14	14.2±0.2	5.0±0.3			
^{98}Mo	87±17	14.2±0.4	4.7±0.4			
^{100}Mo	88±18	13.7±0.2	5.2±0.3			

Table V. Parameters obtained for the isoscalar E3 strength above E_x=15 MeV shown in Figs. 4 and 5. Uncertainties include systematic errors.

				KDE0v1	
Nucleus	% E3 EWSR	m_1/m_0 (MeV)	RMS width (MeV)	m_1/m_0 (MeV)	% E3 EWSR
^{92}Mo	52±7	21.8±0.4	4.3±0.3	26.99	63.85
^{96}Mo	65±9	21.4±0.4	5.8±0.4	26.35	60.66
^{98}Mo	61±8	21.5±0.4	4.2±0.3	26.27	61.01
^{100}Mo	53±7	21.5±0.4	3.7±0.3	26.11	61.80

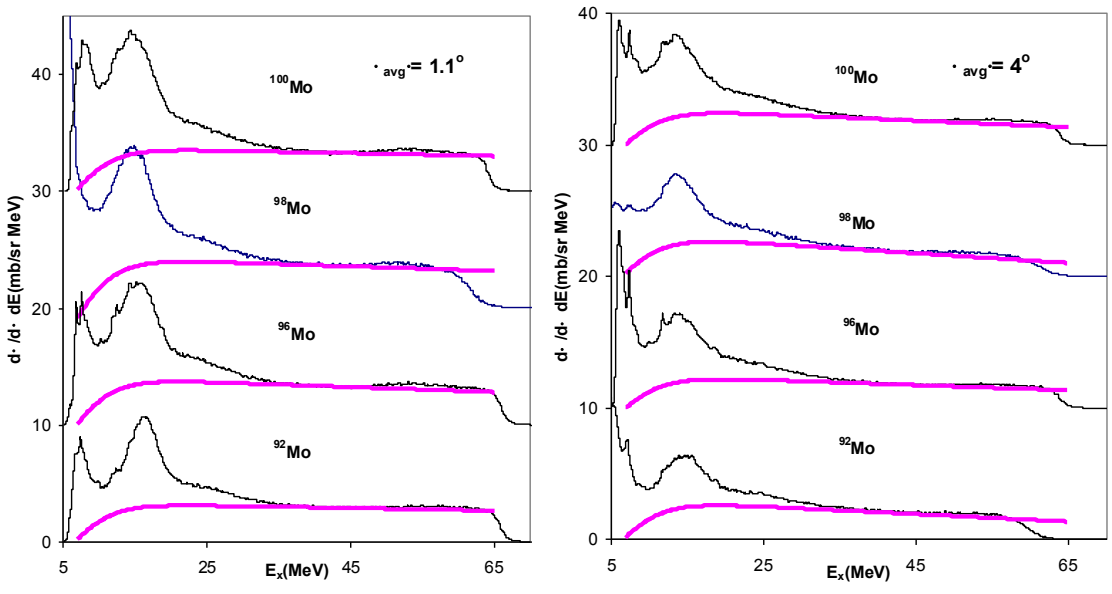

Fig. 1. (Color online) Inelastic α spectra obtained at two angles for ^{92,96,98,100}Mo. The thick pink lines show a continuum chosen for the analysis.

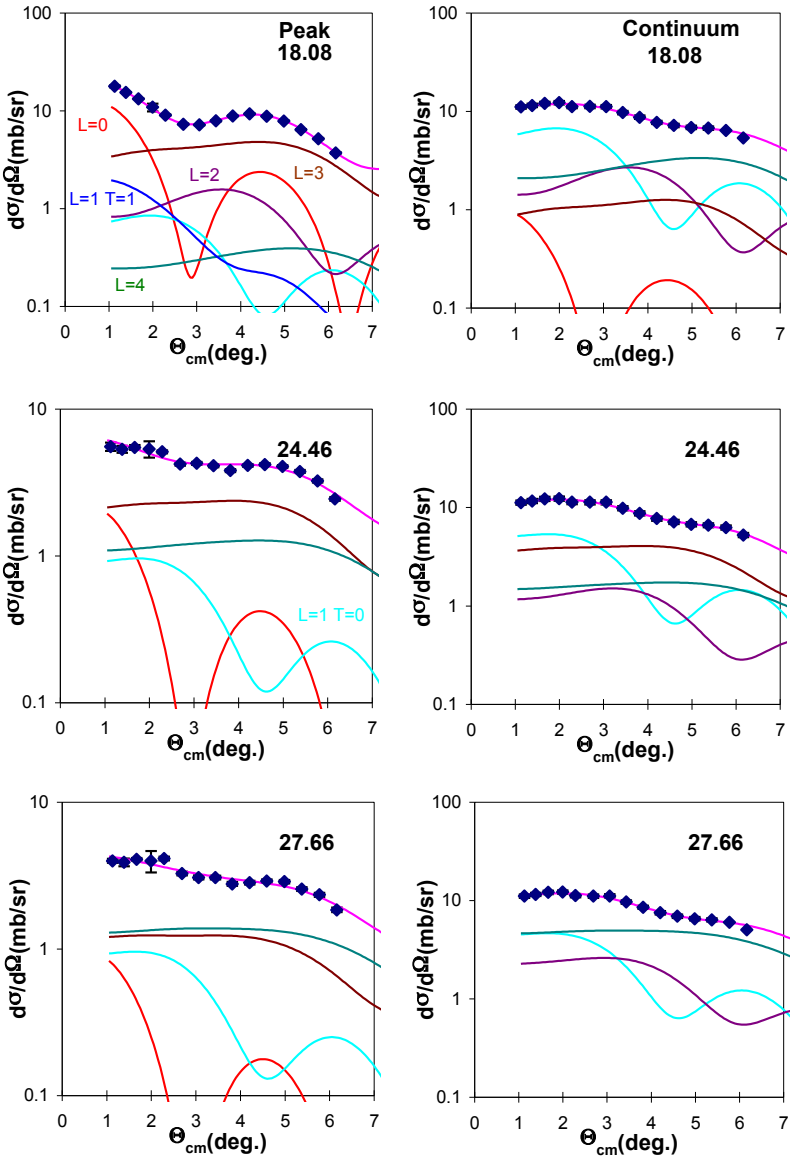

Fig. 2. (Color online) The angular distributions of the ^{92}Mo cross sections for a 500 keV wide bin centered at the excitation energy (in MeV) indicated in each panel for inelastic α scattering for three excitation ranges of the GR peak and the continuum. The lines through the data points indicate the multipole fits. Contributions of each multipole are shown (L=0 red, L=1 T=0 blue-green, L=1 T=1 blue, L=2 maroon, L=3 brown, L=4 green). The statistical errors are shown, but in many cases are smaller than the data points.

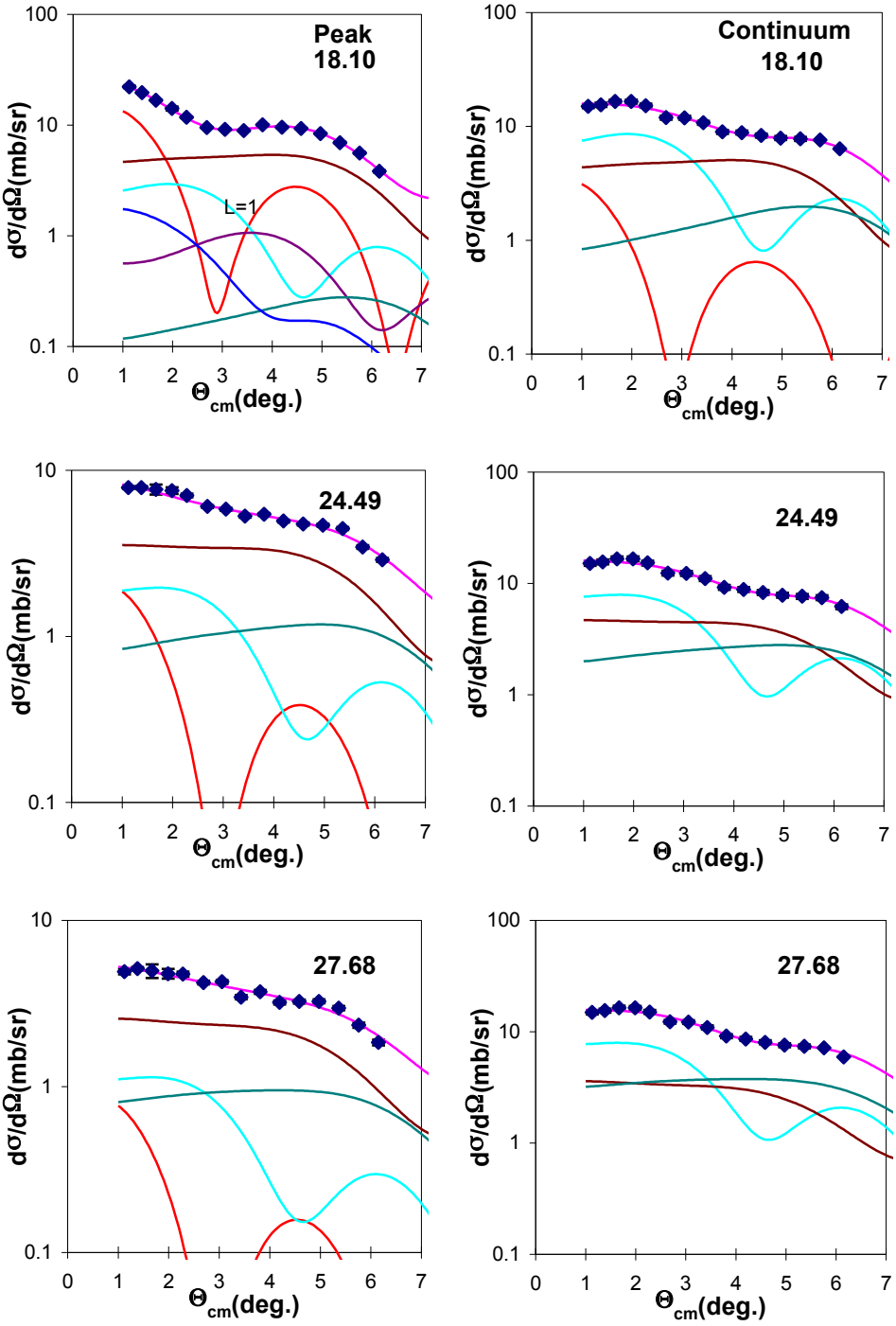

Fig. 3. (Color online) The angular distributions of the ^{98}Mo cross sections. See Fig. 2 caption.

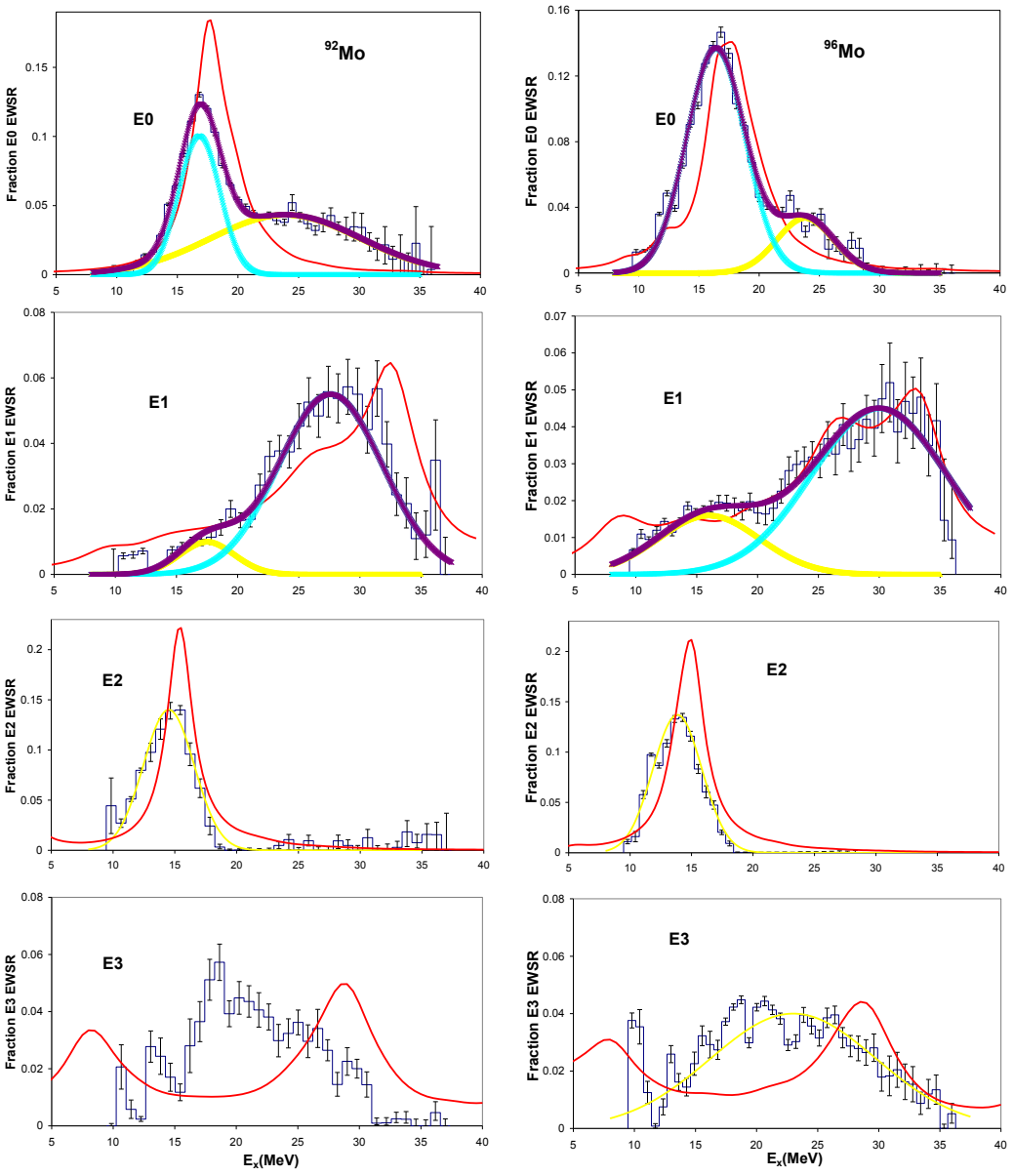

Fig. 4. (Color online) Strength distributions obtained for ^{92}Mo and ^{96}Mo are shown by the histograms. Error bars represent the uncertainty due to the fitting of the angular distributions and different choices of the continuum as described in the text. The thick lines in the E0 and E1 distributions represent the individual peaks and their sum obtained from the Gaussian fits (the blue and yellow lines are the individual peaks, while the brown line indicates the sum). The thin (red) lines are the strength distributions obtained with the HF-RPA calculations using the KDE0v1 interaction, smeared to more closely represent the data as discussed in the text.

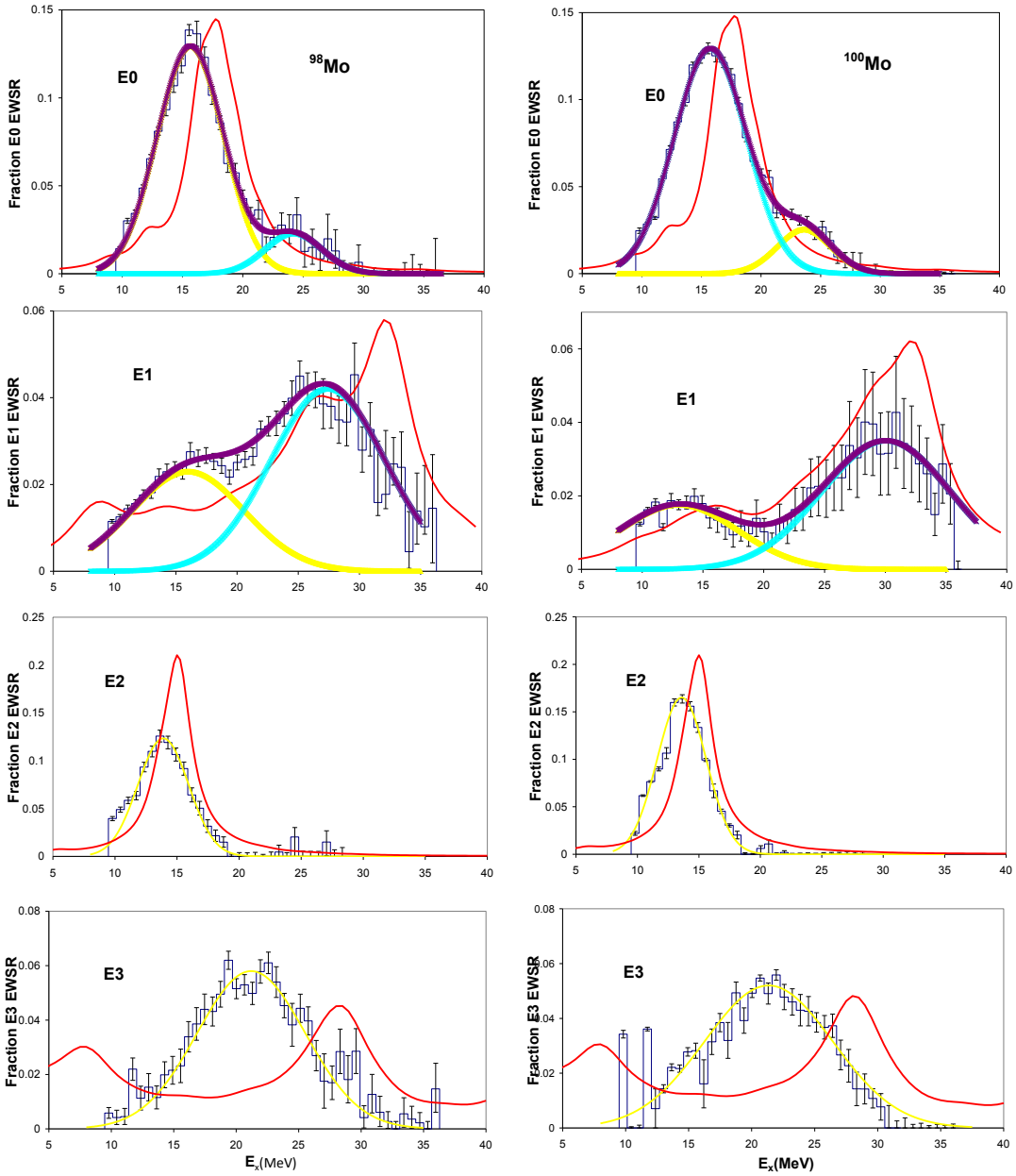

Fig. 5. (Color online) Strength distributions obtained for ^{98,100}Mo are shown by the histograms. See Fig.4 caption.

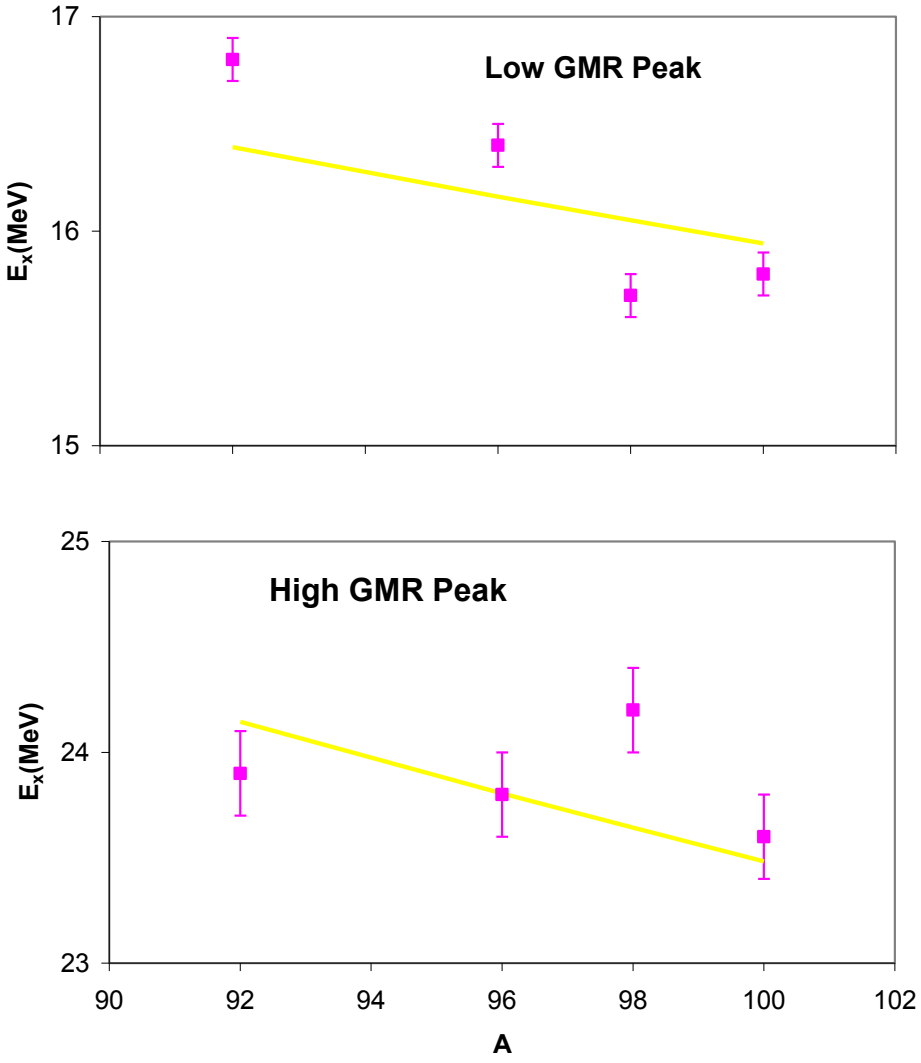

Fig. 6. (Color online) The centroids of the Gaussians obtained from the fits to the E0 distributions for the Mo isotopes are plotted vs. A. The error bars indicate the uncertainty obtained using the errors shown in Figs. 4 and 5. The (yellow) lines show (a) $74*A^{-1/3}$ and (b) $109*A^{-1/3}$ in two plots.

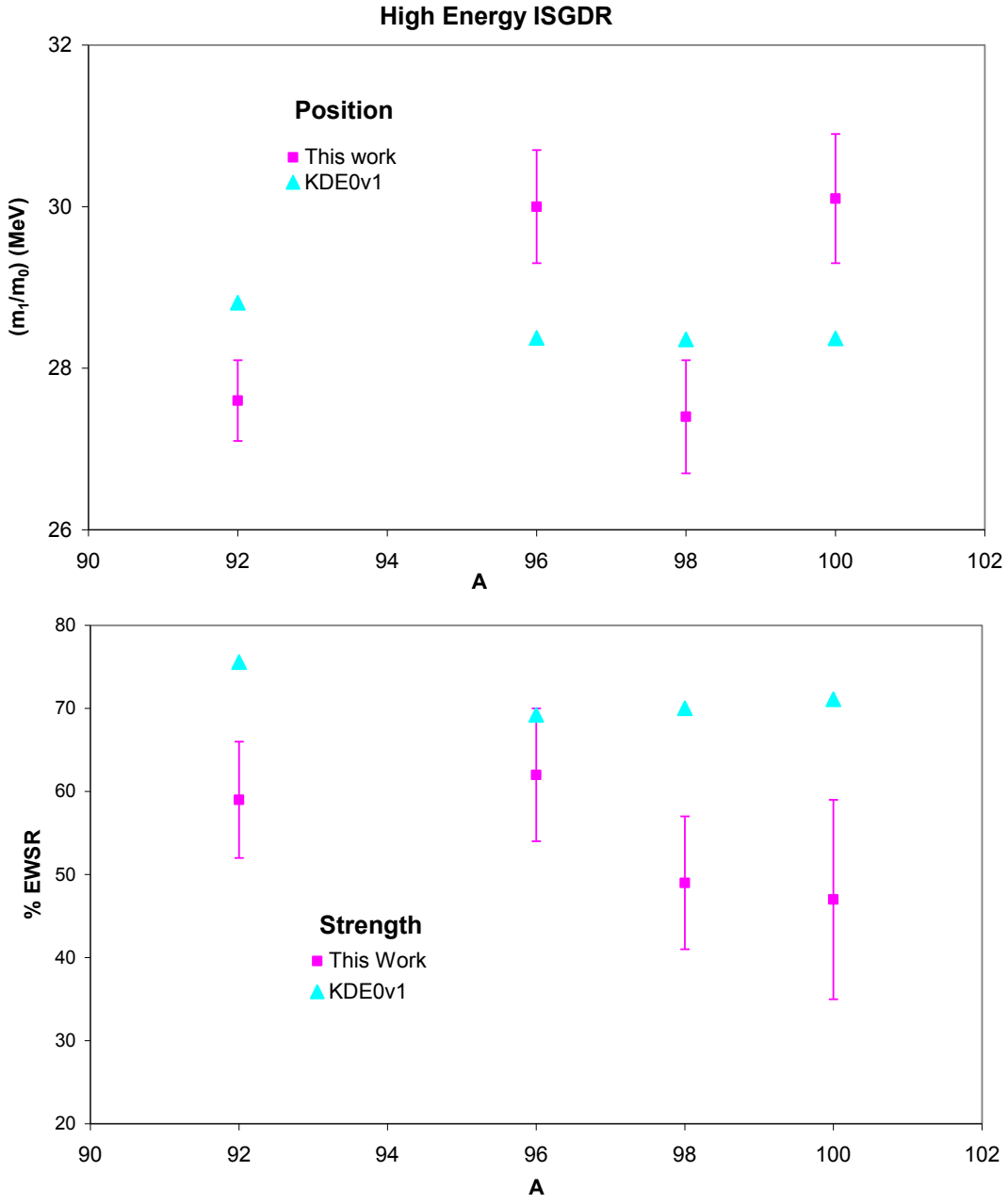

Fig. 7. (Color online) The centroid of the Gaussian fit to the high energy peak in the ISGDR distributions for each of the Mo isotopes is plotted vs. A. in (a) while the strength of the upper peak is plotted in (b). The error bars indicate the uncertainty obtained using the errors shown in Figs. 4 and 5. The triangles (blue) show m_1/m_0 and the strength between E_x=20 MeV and E_x=36 MeV calculated with HF-RPA using the KDE0v1 interaction.

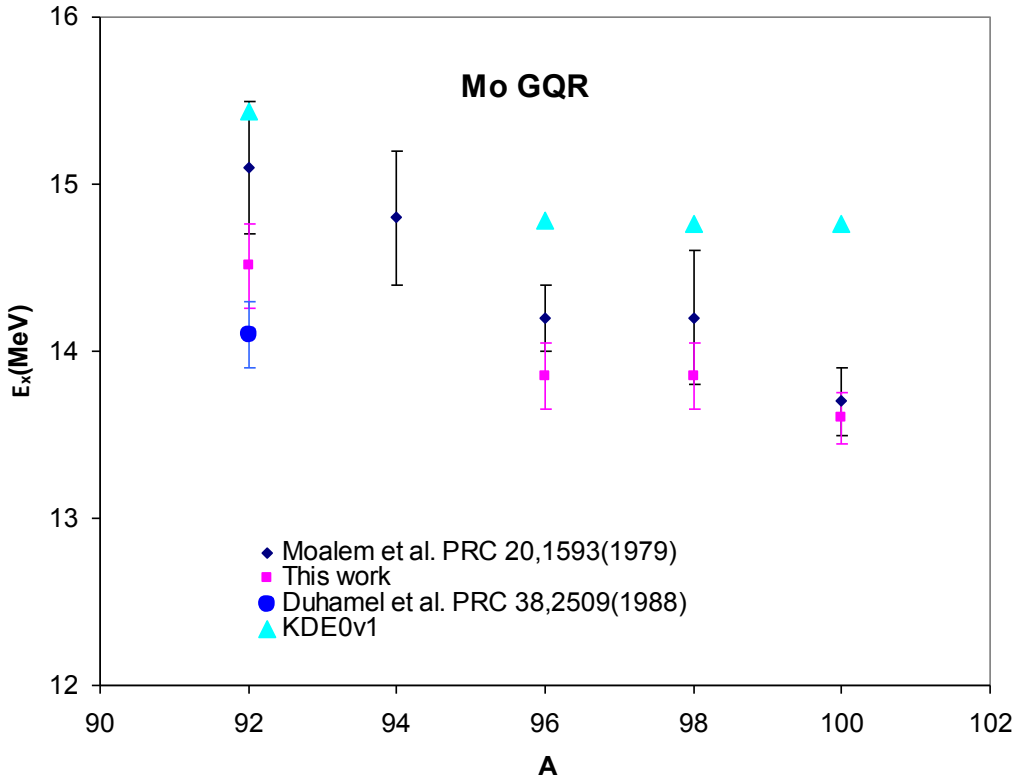

Fig. 8. (Color online) The centroid of the E2 strength in each of the Mo isotopes obtained in this work [red squares] is plotted vs. A. The error bars indicate the uncertainty obtained using the errors shown in Figs. 4 and 5. Also shown with error bars are centroids reported in Ref. [1] (black diamonds) and a measurement for ^{92}Mo [2] (blue circle). The light blue triangles show the centroid of the E2 strength obtained from HF-RPA calculations with the KDE0v1 interaction.

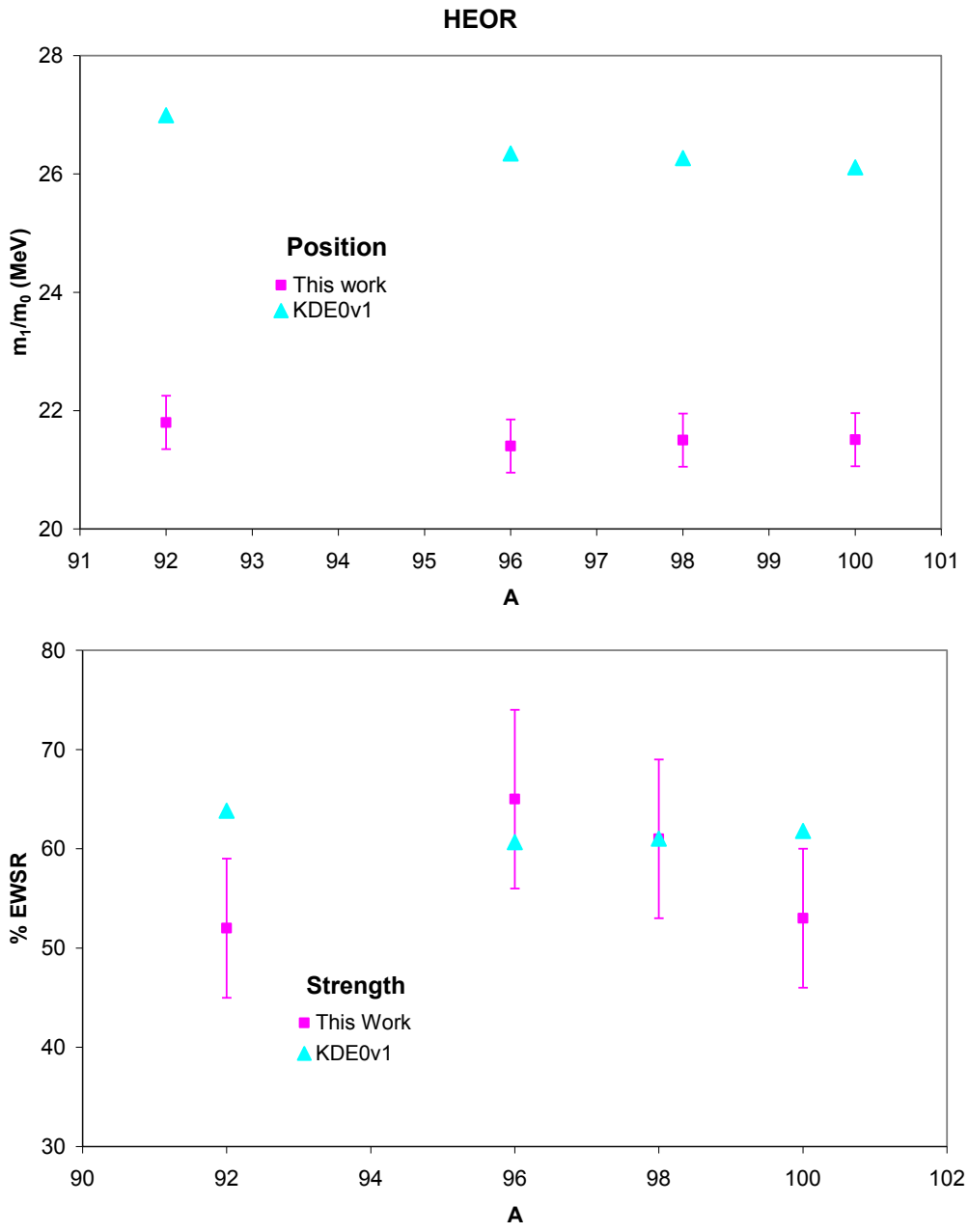

Fig. 9. (Color online) The centroid of the E3 strength observed above E_x=15 MeV for each of the Mo isotopes in this work [red squares] is plotted vs. A in (a), while the strength in this region is plotted in (b). The error bars indicate the uncertainty obtained using the errors shown in Figs. 4 and 5. The large light blue triangles show (a) the centroid and (b) the % EWSR of the E3 strength between E_x=15 MeV and E_x=36 MeV obtained from HF-RPA calculations with the KDE0v1 interaction.